Polymer 51 (2010) 783–792

Contents lists available at ScienceDirect

Polymer

journal homepage: www.elsevier.com/locate/polymer

Comparative study on development of structural hierarchy in constrained annealed simultaneous and sequential biaxially stretched polylactic acid films

X. Ou, M. Cakmak*

Polymer Engineering Department, College of Polymer Engineering and Polymer Science, University of Akron, Akron, OH 44325-0301, USA

ARTICLE INFO

Article history:
Received 14 August 2009
Received in revised form
23 November 2009
Accepted 28 November 2009
Available online 16 December 2009

Keywords:
Poly lactic acid
Heat setting
Biaxial stretching

ABSTRACT

Structural evolution during constrained annealing of PLA films biaxially stretched in simultaneous and sequential biaxial stretching was compared. Annealing of simultaneous biaxially stretched films yields films with in-plane isotropy with (100) crystallographic planes parallel to the surface. The first stage of sequential stretching where the films are stretched in Uniaxial constrained mode was found to yield films exhibiting transverse isotropy. The transverse stretching of these films lead to formation of a distinct second population of chains primarily oriented in transverse direction, generating bimodal orientation texture. When the extent of stretching in two directions are balanced, constrained annealed samples were found to exhibit uniplanar axial (100)[001] texture with the primary chain axial direction now switched to transverse direction. Two new superstructures, along [110] and [100] respectively were discovered in annealed PLA films.

1. Introduction

PLA is an aliphatic polyester with mechanical properties comparable to those of conventional thermoplastics derived from petroleum. It has two main advantages. First, it degrades to lactic acid, which is safe to human being and animals. Second, it can be derived from corn starch, which is a renewable resource [1–4].

Poly L lactic acid has a glass transition temperature(T_g) of 50–60 °C. Its cold crystallization temperature (T_c) ranges between 95 and 105 °C, while its melting temperature(T_m) ranges from 150 to 190 °C [1–3]. ΔH_f of PLA is reported to be 93 J/g [5]. PLA chains have a higher refractive index along chain axis. Intrinsic birefringence of amorphous PLA is found to be 0.03 [1–3]. Crystallizability of PLA determined by its chain regularity and mobility. As the lactic acid is chiral, regularity of PLA chains is significantly affected by the ratio of L component over D component present [6].

PLA exhibits four crystalline forms: α, β, γ and stereo-complex. The orthorhombic α crystal structure is the most commonly observed structure, in which the chains are in −10/3 left helical conformation. Cell dimension of α crystals has been published by several groups. The values provided vary a little from group to group, as: $a = 10.34 \sim 10.7$ Å, $b = 5.97 \sim 6.45$ Å, $c = 27.8 \sim 28.8$ Å [7–10]. Under high stress, β crystal phase with a frustrated crystal structure with trigonal $a = b = 10.52$ Å $c = 8.8$ Å with $P3_2$ space group is formed [11]. More extended 3/1 helical can be observed in this structure. β crystal is found to transform into α crystal when annealed above T_g [7,32]. The triclinic stereo-complex can only be obtained with 1:1 mixture of PLLA and PDLA [12]. The hexagonal γ crystals are grown on a special substrate [13].

Deformation of PLA begins with heating the amorphous precursors to temperatures between glass transition temperature (T_g) and cold crystallization temperature (T_{cc}) where they behave rubbery. The latter cold crystallization temperature is defined as the peak of exotherm observed upon heating from amorphous state. Upon stretching, orientation induced crystallization is eventually induced at certain level of orientation, which depends on the processing conditions including, rate, temperature and mode of stretching [24]. Generally these polymers do not attain high levels of crystallinity and oriented amorphous chains developed in the stretching stage posses long term instability in the use of these films. Typically, these films are optically clear due to very high nucleation rates induced during stretching [1–3]. However, very low crystallinity and crystal perfection are induced at the end of film extension due to the low chain mobility at the stretching temperature. Heat setting or constrained annealing is often the last step in film stretching operations. During this step complex structural reorganization takes place including relaxation, crystallization and crystal perfection. As a result for void healing and internal stress elimination and enhancement of mechanical properties occurs [14–23]. All of the latter phenomena are primarily controlled by the structural details developed during deformation.

* Corresponding author.
E-mail address: cakmak1@uakron.edu (M. Cakmak).

0032-3861/$ – see front matter © 2009 Elsevier Ltd. All rights reserved.
doi:10.1016/j.polymer.2009.11.058

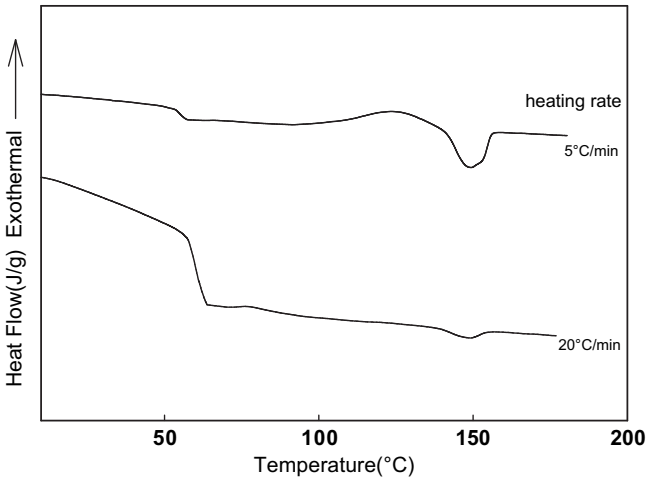

Fig. 1. DSC curve of as cast films.

The biaxial deformation behavior of PLA films was reported in a previous paper [24]. Current paper will focus on structural development during heat setting of PLA films prestretched under simultaneous and sequential deformation modes to contrast the differences arising from these two modes of biaxial stretching.

2. Experimental

Material properties, sample preparation, equipment and experimental procedures employed are described below.

2.1. Material

Linear PLA with number and weight-average molecular weight around 76,200 and 163,600 respectively, kindly provided by Dow-Cargill LLC, was used for this research. 8% D component is randomly distributed in the chains to depress its melting point. As a result, Tm of this material ranges between 145 °C–150 °C. T_g and T_c of this material is found to be around 60 °C and 110 °C respectively. The melt casting conditions adjusted such that the resulting films were free of crystallinity and orientation. Details of the film casting process are given elsewhere [25]. DSC scan confirmed that the crystallinity of as cast film is negligible, as shown in Fig. 1. Both in-plane and out of plane retardation are found to be zero in as cast film.

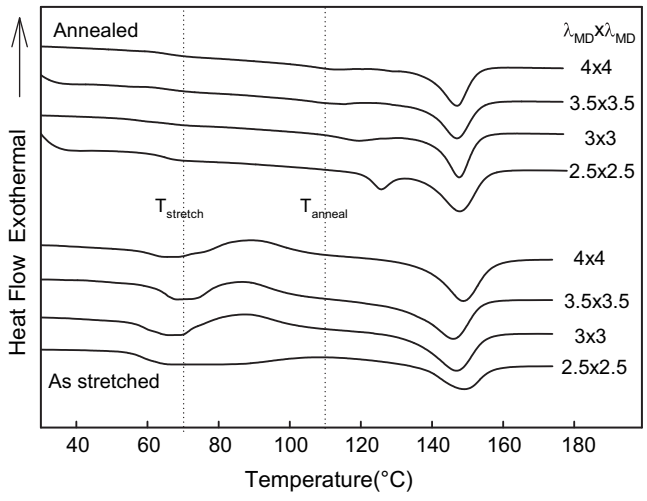

Fig. 2. DSC curves of SB samples.

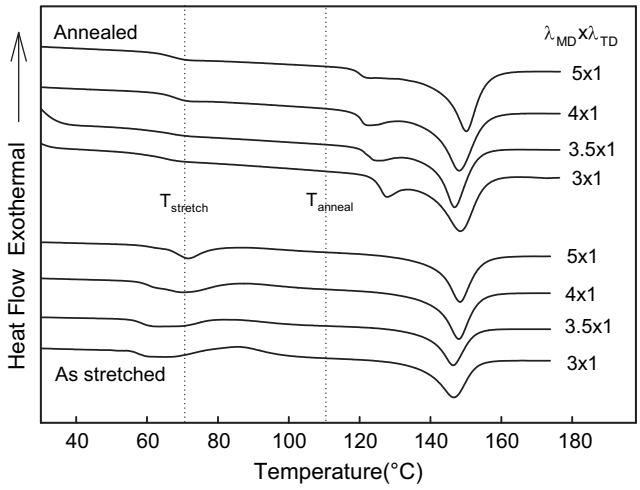

Fig. 3. DSC curves of UCW samples.

2.2. Sample preparation

The amorphous isotropic films were stretched in two modes:

Simultaneous Biaxial (*SB*): the films are extended in two perpendicular directions at the same rate and to the same ratio.

Sequential Biaxial (*SEQ*): the films are extended in Machine direction (MD) in uniaxial constrained width (UCW) mode, after completion of stretch in MD, it is extended in the perpendicular transverse direction (TD) in UCW mode. Same stretching rates were used for both stages of stretching.

All the films reported in this research were stretched in the rubbery state at 70 °C. After completion of stretching process in an Iwamoto 702 biaxial stretcher, the samples were remained in the chamber and constrained by clamps. The chamber of the biaxial stretcher is then heated up to 110 °C in about 8 min. Then, the films are annealed at 110 °C for 20 min. At the end of this process, the films are quenched to below T_g by air cooling before they are removed from the chamber. Samples with very low stretch ratio form uneven wrinkles during the annealing process, thus they are not studied in this research.

2.3. Thermal analysis

Thermal properties of the samples were measured with a Dupont 2920 differential scanning calorimeter in a dry nitrogen

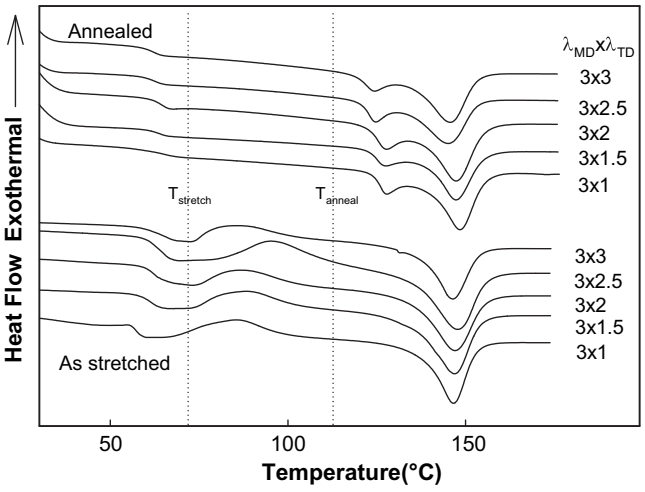

Fig. 4. DSC curves of SEQ samples with $\lambda_{MD} = 3$.

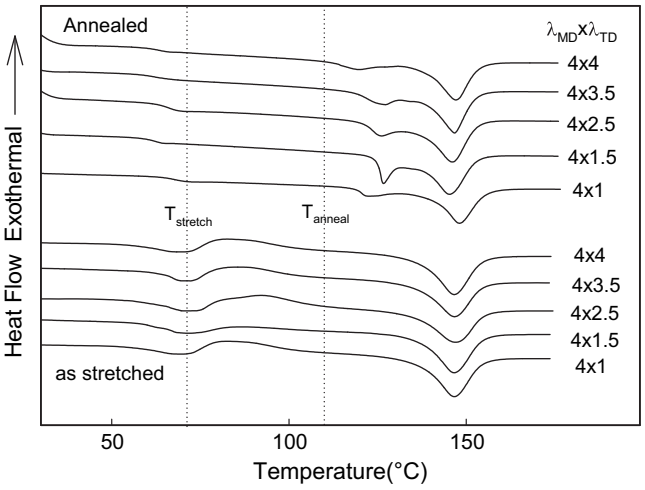

Fig. 5. DSC curves of SEQ samples with $\lambda_{MD} = 4$.

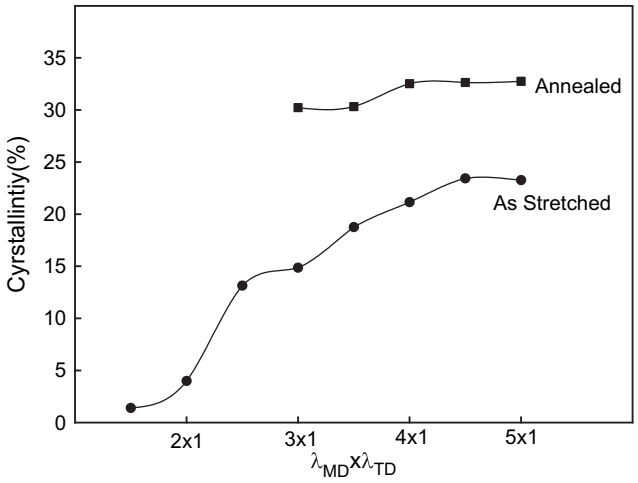

Fig. 7. Crystallinity vs. λ_{MD} of as stretched and annealed UCW samples.

medium using 20 °C/min 0–180 °C range. The samples of 6–10 mg were crimped in standard Aluminum pans.

Crystallinity of the samples are calculated with the equation below:

$$\text{Crystallinity}\ (\%) = \frac{\Delta H_{exp}}{\Delta H_f} \times 100\% \tag{1}$$

Where $\Delta H_{exp} = \Delta H_{metling} - \Delta H_{cold\ crystallization}$, and ΔH_f is the heat fusion of 100% crystalline PLA, which was taken as 93 J/g [5]. The $\Delta H_{cold\ crystallization}$ peak represents that portion of the heat fusion induced by cold crystallization during DSC scan. That portion must be subtracted from the melting peak in order to obtain the material original crystallinity before DSC scan.

2.4. Birefringence

In plane and out of plane birefringence of the samples was measured with a Gaertner Polaroscope with a Babinet compensator. This optical bench contains a goniometer, which enables the sample to be rotated. In plane and out of plane birefringence values are calculated Stein's equations [26]:

$$\Delta n_{12} - \frac{\lambda_0 R_0}{d_0} \tag{2}$$

$$\Delta n_{13} - \frac{\lambda_0}{d_0}\left[\frac{R_0 - R_\varphi\left(1 - \sin^2\varphi/\bar{n}^2\right)}{\sin^2\varphi/\bar{n}^2}\right] \tag{3}$$

$$n = \frac{n_1 + n_2 + n_3}{3} \tag{4}$$

$$\Delta n_{23} = \Delta n_{13} - \Delta n_{12} \tag{5}$$

Where λ_0 is the wavelength of the incident light, d_o is the sample thickness. φ is the tilting angle, R_o is the retardation of the film from blank measurements. R_φ is the retardation of film tilted by angle φ. n represents the average refractive index of PLA, which is taken as 1.47 [27]. 1, 2 and 3 represents MD, TD and Normal direction (ND) respectively.

2.5. Wide angle X-ray diffraction(WAXD)

A Rigaku diffractometer was employed to investigate the changes in the chain conformation in crystalline phase due to processing history. The voltage and current were set to be 150 KV and 40 mA. A $\theta/2\theta$ scan from 27 to 34° was used to locate the peak

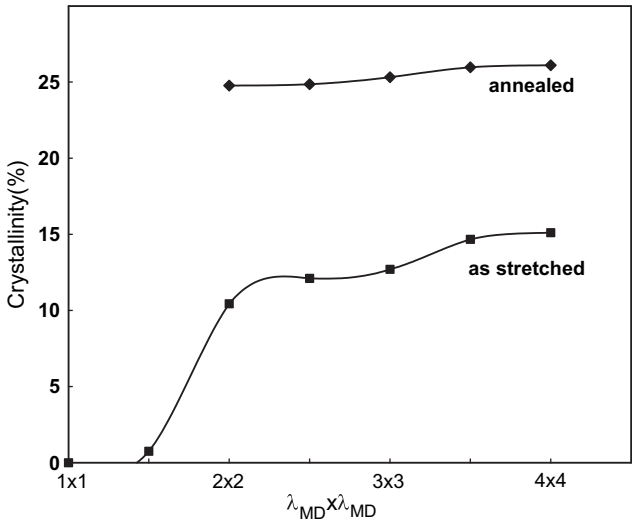

Fig. 6. Crystallinity vs. λ_{MD} of SB Samples.

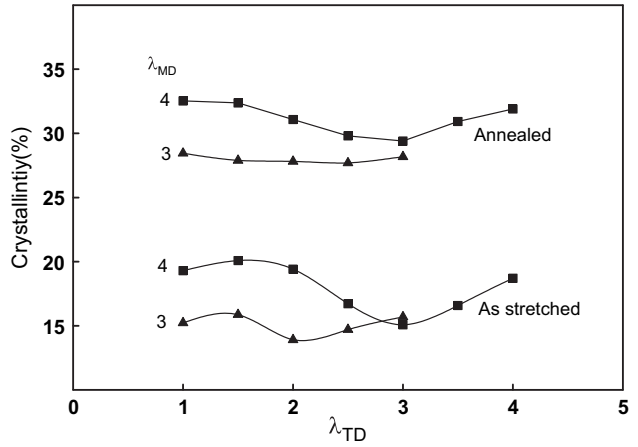

Fig. 8. Crystallinity of SEQ Samples before and after annealing.

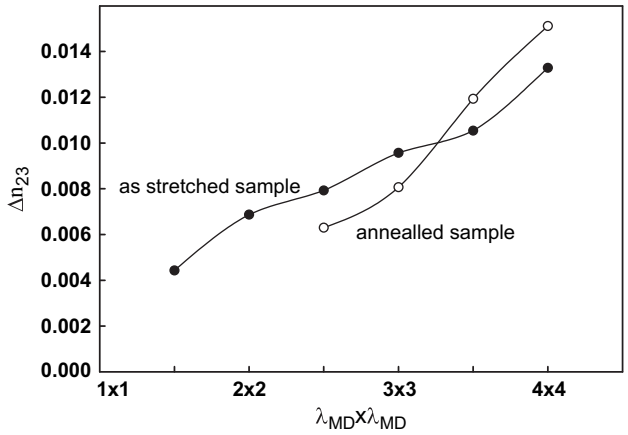

Fig. 9. $\Delta n23$ vs. λ_{MD} of SB samples.

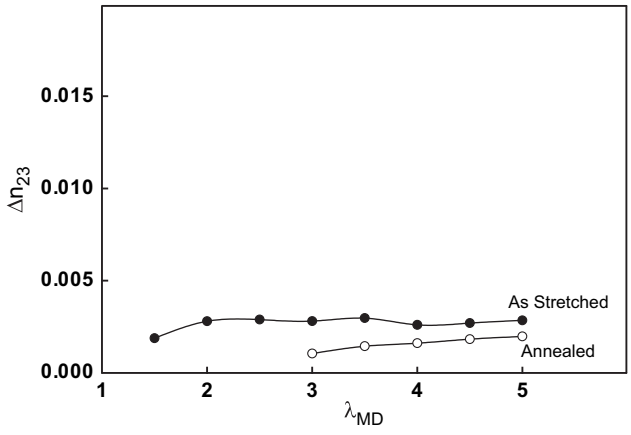

Fig. 11. Δn_{23} vs. λ_{MD} of UCW Samples.

position of (0 0 10), which indicates the helix conformation of PLA chains in crystalline phase. The samples were mounted with MD horizontal to scan only the meridian. Step size of the scan was chosen to be 0.02 and integration time was chosen to be 10 s.

2D WAXS images were obtained using in flat plate geometry using a Rigaku X-ray Image plate system with a 18 KW rotating anode X-ray generator. A 15 min exposure time is required to get high quality pattern. The sample to detector distance was chosen to be 150 mm. The films were carefully stacked to a thickness of 1 ~ 1.5 mm to get WAXS images. The X-ray beam is directed in two directions: ND and MD.

Pole figures of selected samples were obtained with a GE XRD-6 X-ray generator equipped with an automated quarter circle goniometer. Voltage and current of the X-ray tube on this GE X-ray unit was set to 30 KV and 30 mA respectively. For each combination of χ(chi) 5° and φ(phi) 10° step, 10 s integration time was used. The films were stacked to form 4 mm × 1.5 mm × 1.5 mm prism that was mounted on the goniometer with spindle axis parallel with MD. The pole figures of combined crystalline diffractions of the (200) & (110) planes in and/or corresponding diffraction from interchain correlation in amorphous phase were measured.

3. Results and discussion

3.1. Thermal analysis

As shown in Fig. 2, simultaneous biaxial stretching to larger stretch ratios shifts the cold crystallization temperature to lower temperatures but area under the cold crystallization peak does not decrease indicating that the polymer chains become oriented (decrease of T_c) but not crystallized. Annealing at 110 °C eliminates the cold crystallization peak and a secondary melting peak appear in annealed samples about 20 °C above the annealing temperature. This secondary melting peak shifts to lower temperature with increasing λ_{MD} and become a broad shoulder beyond λ_{MD} of 3. A secondary melting peak 10–30 °C above annealing temperature is commonly observed after annealing of slow crystallizing polymers [14–16,23]. During annealing, the imperfect and small crystals melt and re-crystallize into larger and more perfect crystalline state with consequent 10–30 °C rise above the annealing temperature. The increase in λ_{MD}, lead to a tighter crystalline network during stretching. Thus, the chain segments spanning the amorphous phase become less mobile during annealing. The simultaneous biaxially stretched (SB) samples exhibit a broad shoulder, instead of a secondary melting peak when annealed after large deformation λ_{MD}. As expected, glass transition becomes less significant after annealing, as more restriction is applied to the segments in amorphous chains after extensive crystallization.

Similar behaviors are observed in DSC curves of annealed UCW samples, as shown in Fig. 3. A secondary melting peak becomes smaller and shifts to lower temperature with increase in λ_{MD}.

Sequential biaxially stretched samples exhibit quite unique thermal behavior. The sample with 3 × 1 deformation history shows the lowest cold crystallization peak in Fig. 4. The increase of TD stretching actually increases the position of this peak up to 3 × 2.5 where it reverses this trend and decreases. The decrease of

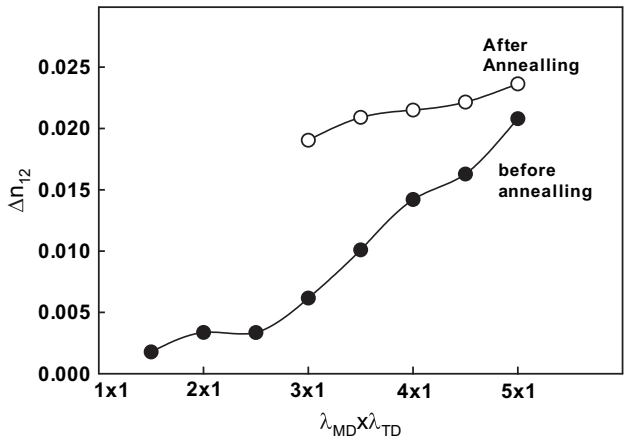

Fig. 10. Δn_{12} vs. Stretch Ratio of UCW samples.

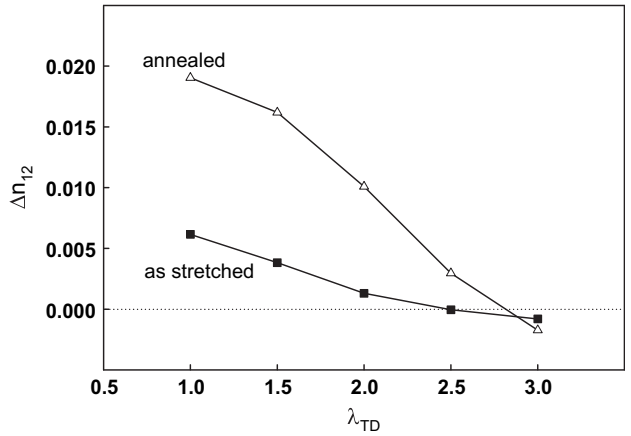

Fig. 12. Δn_{12} vs. λ_{TD} of SEQ with λ_{MD} of 3.

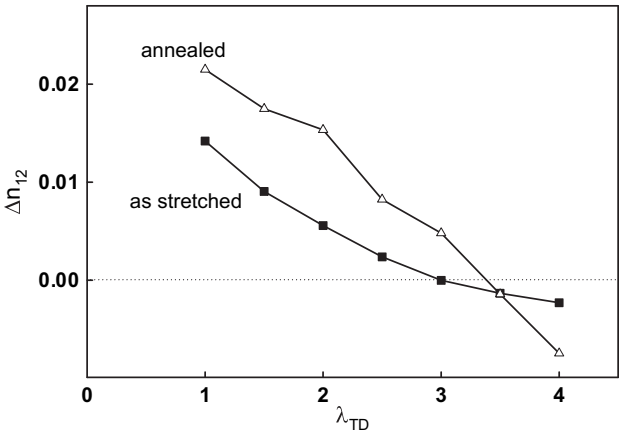

Fig. 13. Δn_{12} vs. λ_{TD} of SEQ with λ_{MD} of 4.

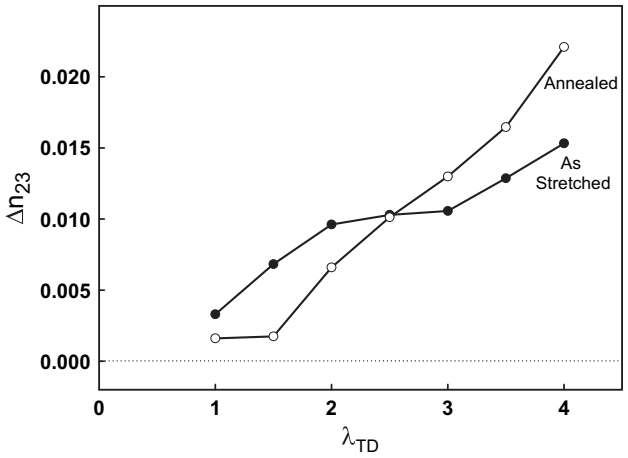

Fig. 15. Δn_{23} of SEQ Samples with λ_{MD} of 4.

cold crystallization peak position is associated with the increased preferential orientation of polymer chains in the amorphous state leading to crystallization at lower temperatures as a result of reduced entropy. Transverse stretching certainly act in opposite direction. As illustrated in Fig. 4, the increase in TD stretching leads to increase of cold crystallization temperature and broadening of the associated peak though these two parameters show reversal at the balanced biaxial stretching state. Upon constrained annealing, the secondary melting peak appears about 20 °C above the annealing temperature and moves to slightly lower temperatures beyond 3×2 deformation. Clearly the size of the secondary melting peak at lower temperature is big. This could be related to the breakup of the crystalline network formed in first stretching direction, creating large amount of nuclei in the film.

After stretching to high λ_{MD}, the transverse stretching clearly disorient the amorphous chains and also increases their fraction as evidenced by the increase of area under the cold crystallization peak and its shift to higher temperature up to 4×2.5 (Fig. 5) beyond this point the peak position reverses its trend. However, the area under the cold crystallization remains high (chains remain oriented but uncrystallized). Annealing of these films creates the secondary melting peak. However the largest increase is observed in the 4×1.5. Subsequent TD stretching reduces the area under these peaks and shift closer to annealing temperature.

Crystallinity of all the samples increased significantly after constrained annealing, as shown in Figs. 6–8. Similar crystallinity is found in all the annealed SB and UCW samples. Obviously, more extensive crystallization occurred in samples with lower λ_{MD}. This can be explained by the fact that the chains that are part of the long range connected network becomes less mobile crystalline network is formed after higher λ_{MD} is reached. Since the annealing temperature employed in this research is much lower than the melting temperature of PLA, the network developed during stretching remains intact during annealing and it tends to lock the chain segments in amorphous phase in configurations unfavorable to crystallization, preventing them from registering into crystalline phase, leading to less extensive crystallization. Similar behavior has been observed in PET [16,17].

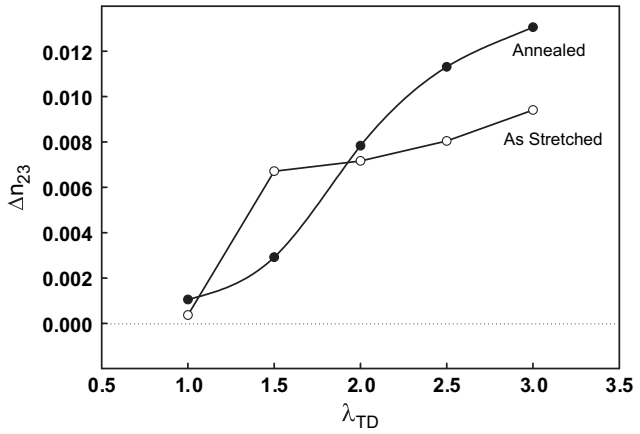

Fig. 14. Δn_{23} vs. λ_{TD} Curves of SEQ Samples with λ_{MD} of 3.

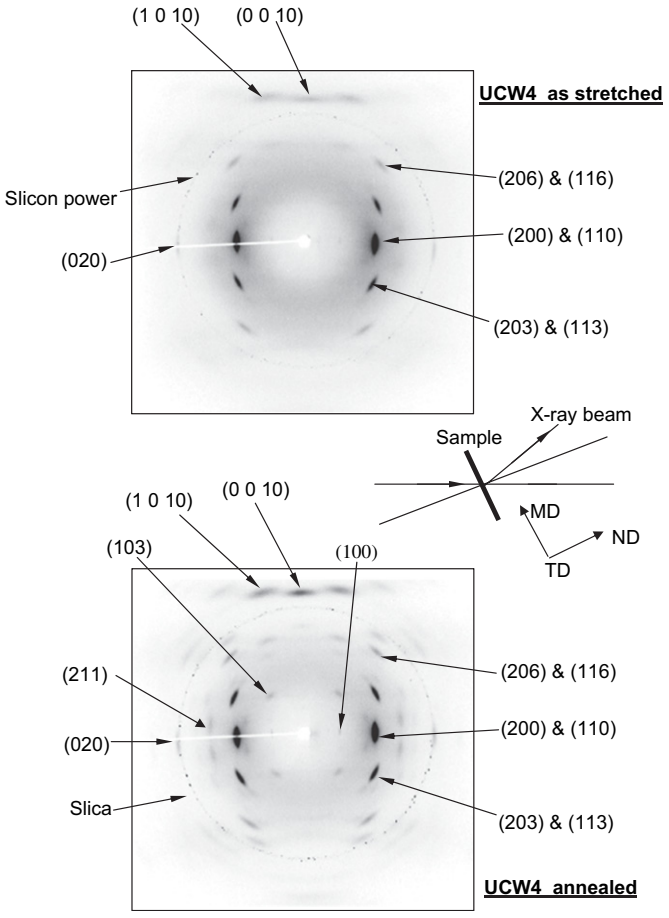

Fig. 16. WAXD patterns of as stretched and annealed UCW4 samples.

Annealed sequential biaxially stretched (SEQ) samples with λ_{MD} of 3 posses similar crystallinity regardless of λ_{TD}. (Fig. 8) While crystallinity of annealed SEQ samples with λ_{MD} of 4 first decreases, and then increases with the increase of λ_{TD}. This is attributable to higher λ_{MD} leads to a more developed crystalline network, enhancing the efficiency of transverse stretching. Thus the crystalline phase is destroyed during transverse stretching, while higher λ_{TD} induce another crystalline phase oriented in TD, leading to recovery in crystallinity [24].

3.2. Birefringence

As expected, in-plane birefringence Δn_{12} of SB sample is found to be very close to zero both before and after annealing confirming the in-plane isotropy in these simultaneous biaxially stretched films (data not shown).

The out of plane birefringence SB samples increases with deformation and annealing has small effect on this birefringence as illustrated in Fig. 9.

In the first leg of the sequential biaxial stretching, the samples are stretched in uniaxial constrained width mode. In plane birefringence rapidly increase beyond about 2.5×1 and continuously increase nearly linearly with deformation after this point. (Fig. 10) Annealing certainly increases the birefringence but the difference between as stretched and annealed samples decrease with increasing deformation. As the as stretched samples develops crystallinity and accompanying structural constraints through formation of long range network, the structural (orientation, crystallinity) changes in the ensuing annealing step becomes less. In the annealing process, rearrangement of segments and extensive crystal growth are increasingly restricted by this network. Out of plane birefringence Δn_{23} remains measurable but nearly constant with deformation as illustrated in Fig. 11.

Stretching in the transverse direction reduces the in-plane birefringence on samples previously stretched to λ_{MD} of 3 as shown in Fig. 12. Zero in-plane birefringence is attained at 3×2.5 condition and stretching to balanced biaxial (3×3) condition leads to negative in-plane birefringence. Annealing, though substantially increases this birefringence, does not change the latter behavior. Out of plane birefringence increases with TD stretching though the differences between as stretched and annealed counterparts is less pronounced than in Δn_{12}.

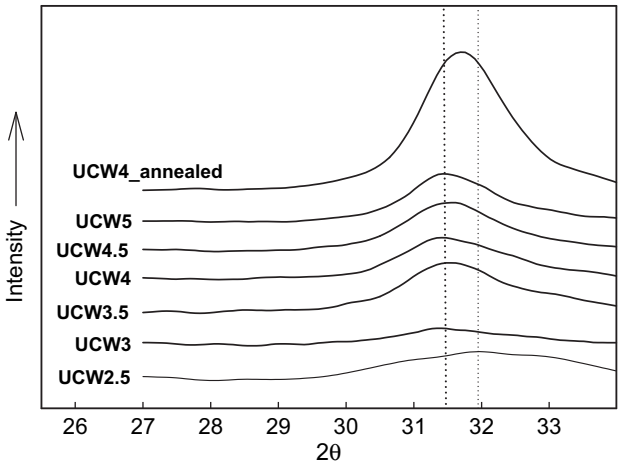

Fig. 18. X-ray profile of UCW samples obtained with $\theta/2\theta$ diffraction method.

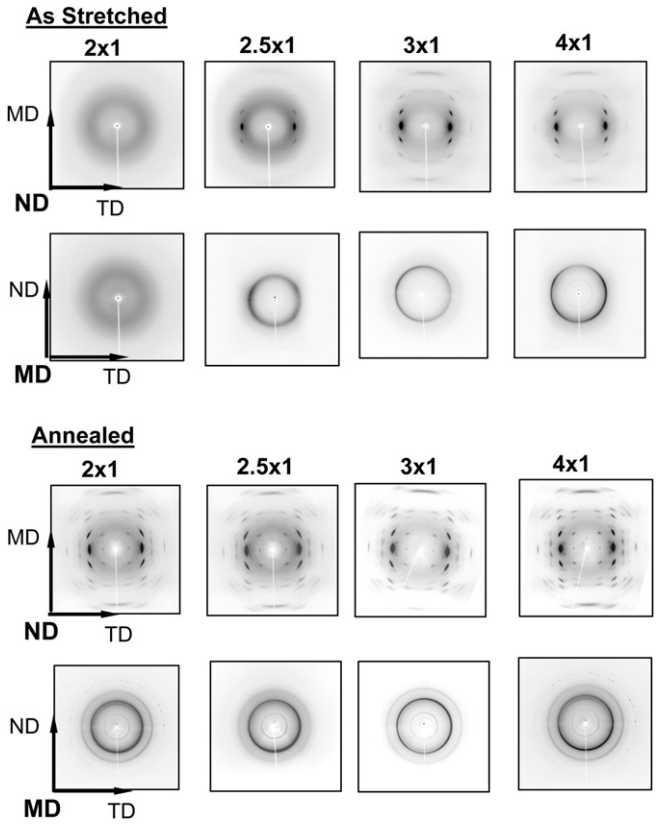

Fig. 17. WAXD images of UCW samples.

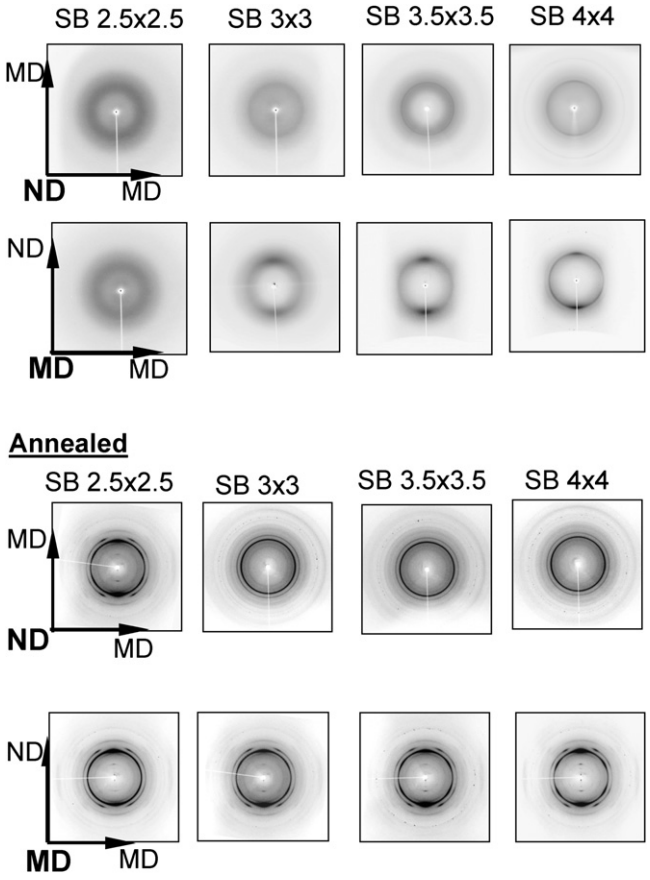

Fig. 19. WAXD images of as stretched and annealed SB Samples.

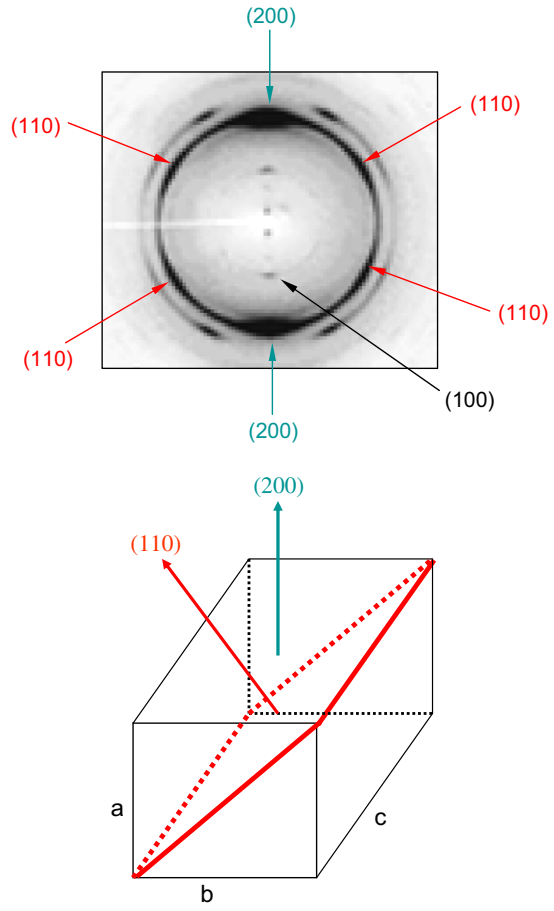

Fig. 20. Orientation of (200) and (110) in annealed SB samples with high λ_{MD}.

Increasing the λ_{MD} to 4 and subjecting the films to a series of TD stretching results in sharp decline in in-plane birefringence as observed earlier and in plane isotropy ($\Delta n_{12} = 0$) is obtained at (4×3) condition. What is interesting is that the Δn_{12} of balanced SEQ samples with λ_{TD} of 4 became much more negative after annealing (Fig. 13).

SEQ samples with low λ_{TD} showed lower Δn_{23} after annealing, while samples with high λ_{TD} showed higher Δn_{23} after annealing, as shown in Figs. 14 and 15. At low λ_{TD}, the network formed during stretching is more or less transversely isotropic. Rearrangement of chain axis is not confined within the film plane, leading to lower Δn_{23} after annealing. After high λ_{TD} is reached, the chains become parallel in the film plane, restricting extensive crystallization and rearrangement of chain axis in the plane of the film, leading to higher Δn_{23} after annealing.

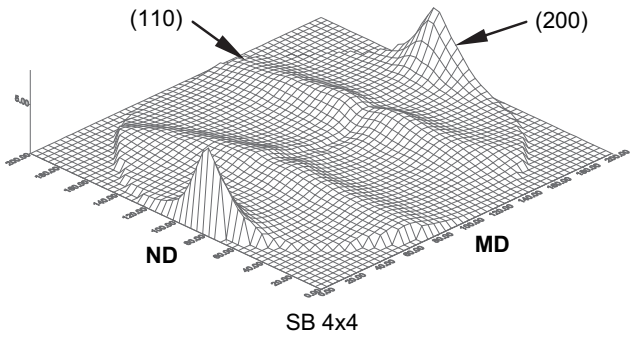

Fig. 21. Pole figure of (200) & (110) of annealed SB sample.

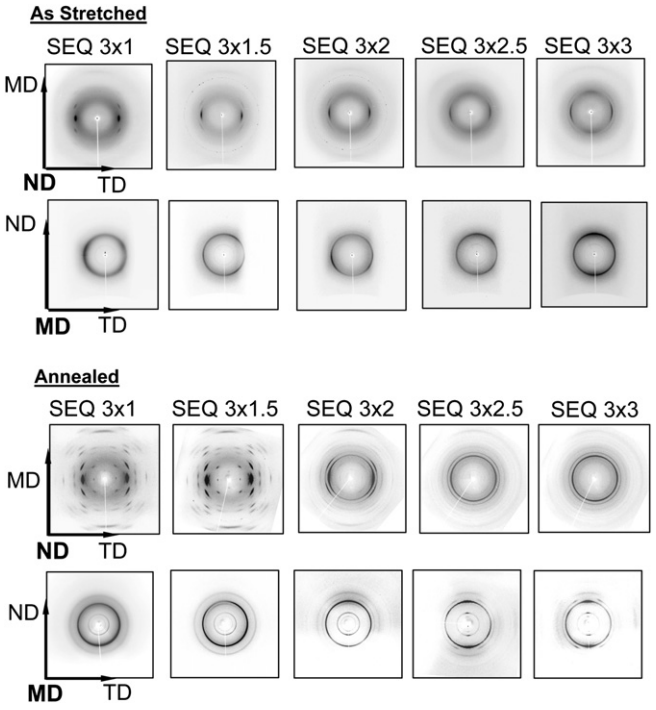

Fig. 22. WAXD images of SEQ samples with λ_{MD} of 3.

3.3. WAXD

WAXD image of as stretch and annealed UCW4 samples obtained through ND and MD are compared in Fig. 16 shows the close up view of two patterns on as stretched and annealed films with all the crystalline peaks identified. Fig. 17 show the WAXS patterns taken with X-ray beam along the normal direction and along the machine direction. The orientation of crystals along MD

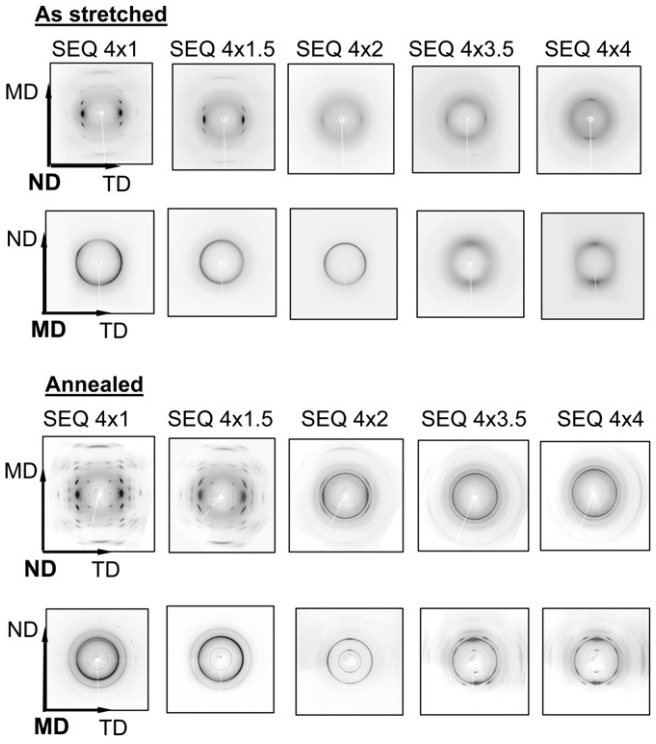

Fig. 23. WAXD images of SEQ samples with λ_{MD} of 4.

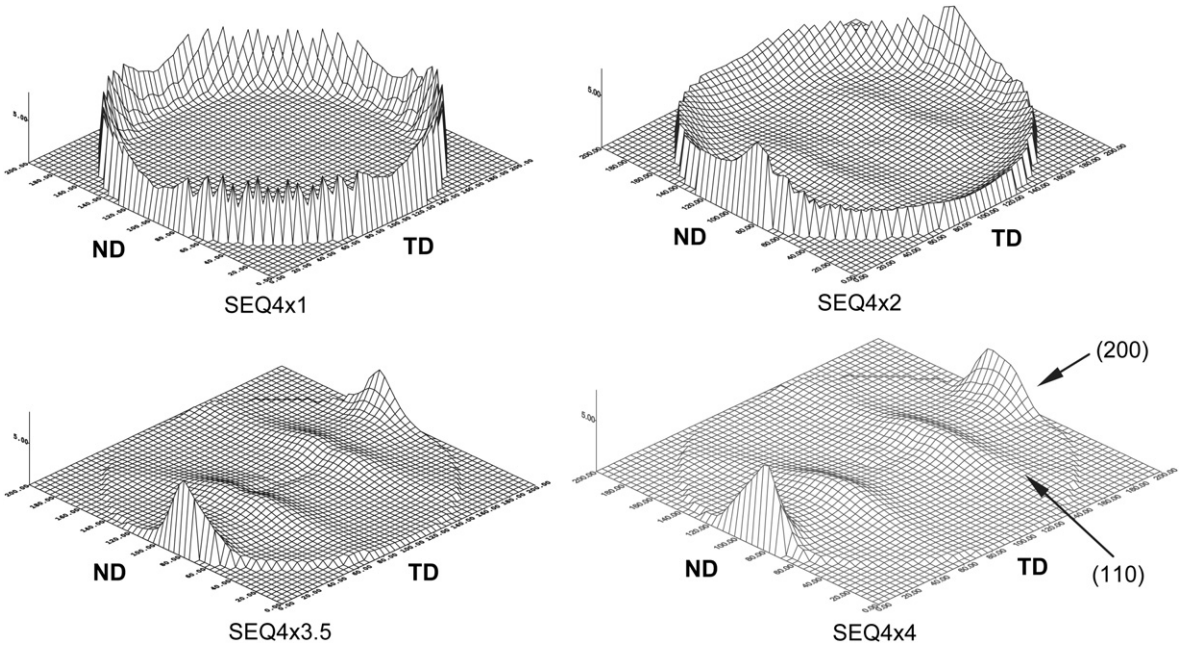

Fig. 24. Pole figure of (200) & (110) of annealed SEQ sample.

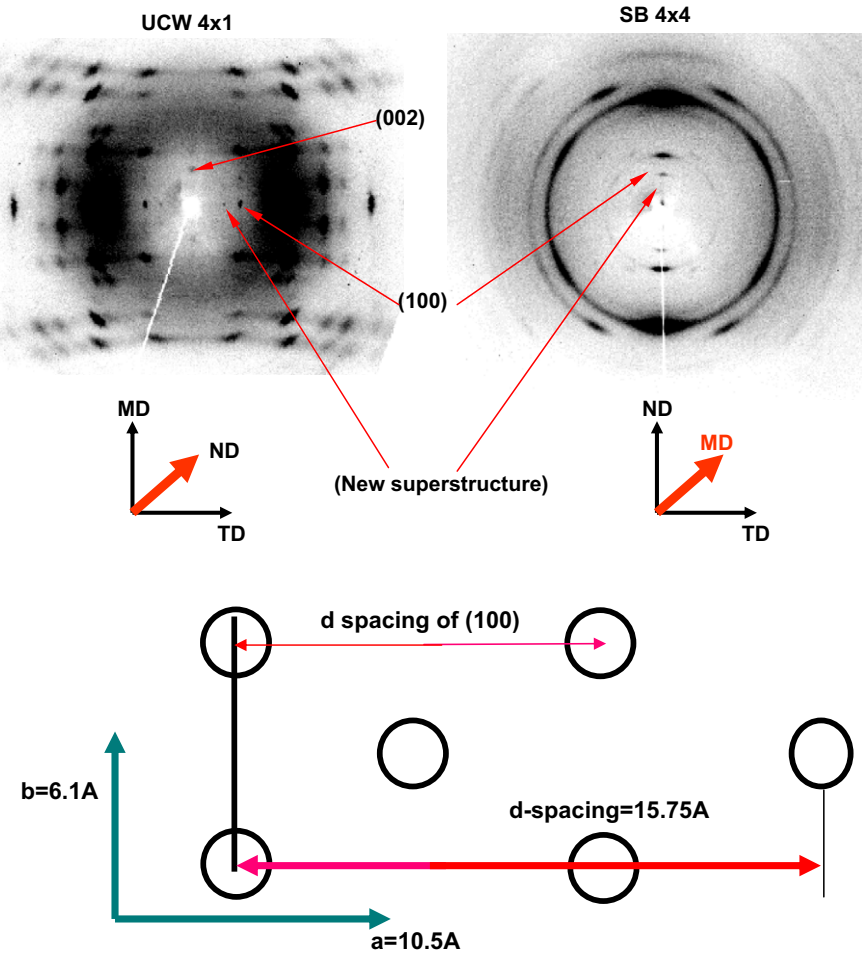

Fig. 25. New structure along [100] direction.

and transverse isotropy are preserved during annealing. Definition and number of crystalline diffraction peaks increases in annealed samples, indicating the fact that the distorted imperfect crystals are transformed into perfect α crystals during annealing process [24]. The diffraction peak of (0 0 10) shifts to a higher 2θ value (Fig. 18) upon annealing, indicating retraction of chain helix during annealing. Obviously the chains (and helices) are extended under stress during stretching processing. During constrained annealing, they undergo retraction and crystallization.

In plane isotropic orientation of crystals is observed in annealed SB samples, as shown in Fig. 19. In the images obtained through MD of annealed SB samples with high λ_{MD}, six concentrations of intensity can be observed in the diffraction plane that is a combination of (200) and (110) planes that exhibit same d-spacing. Besides the two strong meridional concentration, another four weaker peaks 60° from meridian can be observed (Fig. 20). Since meridian concentration of (100) is clearly observable, indicating that a-axis is perpendicular to film plane, it is safe to claim that the two strong meridian concentrations correspond to (200). From the lattice structure, it can be deduced that the angle between (200) and (110) is 60°. So, the weaker concentrations correspond to (110), as shown in Fig. 20. This indicates that (200) is highly parallel with the film plane, leading to separation of (200) and (110) in WAXD pattern. Similar behavior is observed in diffraction of (203) and (113) planes.

To further clarify the orientation of crystals in annealed SB samples, pole figure of (200) & (110) are obtained. (Fig. 21) It is seen that intensity of (200) concentrate in ND and intensity of (110) formed a uniform intensity ridge. Apparently, a uniplanar orientation, with c-axis randomly oriented in film plane and (200) parallel with film plane, exists in annealed SB samples [28–32].

As shown in Figs. 22 and 23 the films stretched in uniaxially constrained width mode exhibit very high orientation in crystalline domains. Though there is some three dimensional order developed as evidenced by the presence of some off-equatorial peaks, it is not very well developed. Application of transverse stretching in $\lambda_{MD} = 3$ (Fig. 22) gradually develops a second population of polymer chains oriented in TD with poorer structural order (please note in 3×3 WAXS pattern), diffraction peak width for (110)(200) combination peak developed in meridian is broader in comparison with that of original equatorial peak. Constrained annealing significantly develops long range order as evidenced by the appearance of large number of diffraction peaks in the WAXS pattern. The bimodal orientation developed during stretching in balanced biaxially stretched film is preserved upon annealing though azimuthal spread of (110)(200) combination peak increases with annealing. If the films stretched to $\lambda_{MD} = 4$, transverse stretching significantly damages the crystalline regions (Fig. 23) and bimodal orientation become observable at an unbalanced stretching state (4×3.5) and in balanced biaxial condition (4×4) exhibit higher population of preferentially oriented chains in the transverse direction. Constrained annealing was found to substantially enhance the crystalline order.

From the WAXD pattern obtained with X-ray beam along MD, we can see that transverse stretching first induce meridional concentration of (100) plane, which is superimposed on a uniform intensity ring, in annealed samples. This shows that some crystals posses parallelism between (100) and film plane while others are still in uniaxial orientation with transverse isotropy. In annealed sample with high λ_{TD}, six peaks on innermost diffraction ring of (200) and (110) in SEQ samples are found, indicating high parallelism between (200) and film plane.

To further illustrate the orientation of crystals after annealing, pole figure of (200) and (110) planes are obtained. (Fig. 24) we can see that (hk0) is uniformly distributed in annealed UCW sample, indicating uniaxial orientation of crystals with *c*-axis oriented in

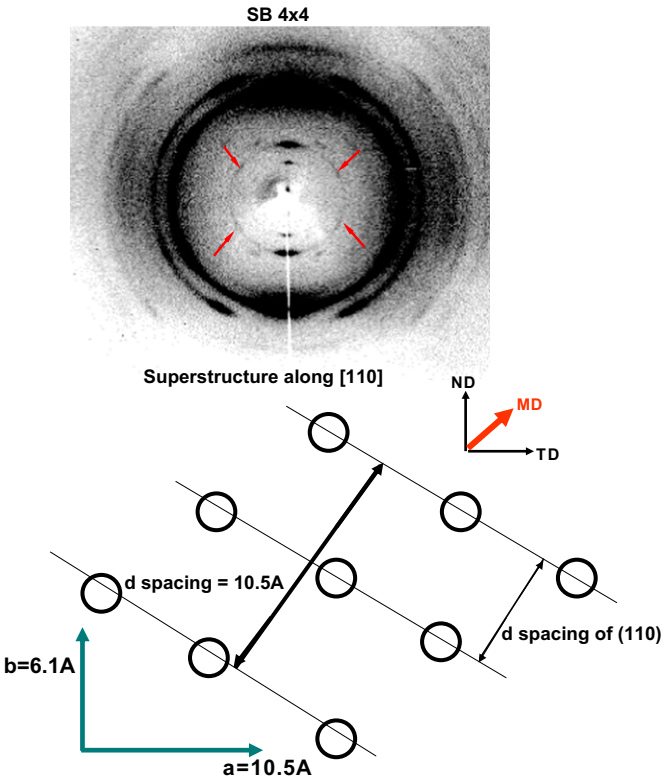

Fig. 26. New superstructure along [110] direction.

MD and transverse isotropy. At the initial stage of transverse stretching, it tends to induce some parallelism between (200) and film plane as indicated by concentration of intensity in ND, while most of the intensity is still uniformly distributed. Apparently, two populations exist in the sample. One posses a uniplanar axial orientation with *c*-axis oriented in MD and (200) parallel with film plane, another still posses a uniaxial orientation. Further transverse stretching tends to enhance the parallelism between (200) and film plane. At balanced biaxial condition, *c*-axis become preferentially oriented in TD as indicated by the concentration of (110) diffraction, forming a uniplanar axial orientation of crystals with c-axis oriented in TD and (100) parallel with film plane.

Two superstructures are observed along [100] and [110] respectively, as indicated in Figs. 25 and 26. By increasing the contrast of WAXD pattern of annealed UCW samples obtained through ND, a (hk0) diffraction at very low 2θ can be observed. By checking the WAXD image of annealed SB sample obtained through MD, it is seen that this new structure is parallel with (100) plane. The d-spacing of this structure is 15.75 Å, which is about 1.5 times of an axis. Upon further increase of contrast further reveals four weak concentrations at 60° from meridian in WAXD pattern of annealed SB sample obtained through MD. (Fig. 26) Apparently, this structure is parallel with (110) plane and its d-spacing is the same as (100), which is twice as long as the d-spacing of (110).

4. Conclusions

Constrained annealing of as stretched films leads to enhancement of structural order by increasing crystal size and perfection and crystalline fraction regardless of deformation mode and extension. The extended helical chain conformation developed during stretching was found to relax by reducing the pitch upon constrained annealing. The general symmetry developed during stretching was found to be preserved upon annealing: UCW

stretched samples exhibit uniaxial symmetry. Simultaneous biaxial stretching consistently develops films with in-plane isotropy. Upon annealing (100) uniplanar texture was found to dominate in these SB films. The type of texture developed in sequentially biaxially stretched films depends on extent of stretching in MD as well as TD. The samples with low λ_{TD} exhibit uniaxial symmetry. The unbalanced biaxially stretched samples exhibit bimodal (cross-hatched) orientation distribution at intermediate and balanced biaxial deformation stages. Dominant texture in the annealed counterparts was found to be (100)[001] texture with (100) planes preferentially oriented parallel to the film plane and chain axes are either preferentially in MD at low TD stretch ratios or in TD at balanced biaxially stretched conditions where the films are found to exhibit unbalanced in-plane properties including birefringence. At high deformation levels, the in plane isotropy in sequential biaxially stretched samples could only be attained in unbalanced biaxial deformation conditions. We also observed two new superstructures along [100] and [110] respectively.

References

[1] Datta R, Tsai SP. FEMS Microbiol Rev 1995;16:221.
[2] Lunt J. Polym Degrad Stab 1998;59:142.
[3] Garlotta D. J Polym Environ 2002;9:63.
[4] Amass AJ, N'Goala KLR, Tighe BJ, Schue F. Polymer 1999;40:5073.
[5] Fischer EW, Sterzel HJ. Kolloid-Zeitschrift und Zeitschrift für Polymere 1973;251:980.
[6] Kister G, Gassanas G. M vert Polym 1998;39:267.
[7] Hoogsteen W, Postenma AR. Macromolecules 1990;23:634.
[8] De Dantis P, Kovacs AJ. Biopolymers 1968;6:299.
[9] Kalb B, Pennings AJ. Polymer 1980;21:67.
[10] Kobayashi J, Asahi T. J Appl Phys 1995;77:2957.
[11] Puiggali J, Ikada Y, Tsuji H, Cartier L, Okihara T, Lotz B. Polymer 2000;41:8921.
[12] Okihara T, Tsuji Masaki. J Marcromol Sci Phys Ed 1991;B30:119.
[13] Cartier L, Lotz B. Polymer 2000;41:8909.
[14] Greener J, Tsou AH, Blanton TN. Polym Eng Sci 1999;39:2403.
[15] Gohil RM. J Appl Polym Sci 1994;52:925.
[16] Lee KG, Schultz JM. Polymer 1993;vol. 34:4455.
[17] Maruhashi Y, Asada T. Polym Eng Sci 1992;32:481.
[18] Varma Pankaj, Lofgren EA, Jabarin SA. Polym Eng Sci 1998;38:245.
[19] Golden JH, Hammant BL, et al. J Appl Polym Sci 1967;11:1571.
[20] Brady TE, Yeh GSY. J Macromol Sci Phys 1993;B7(2):243.
[21] Blundell DJ, Keller A, Kovacs AJ. J Polym Sci 1966;B4:481.
[22] Tian M, Loos Joachim. J Polym Sci Part B 2001;39:763.
[23] Choi J, Cakmak M. ANTEC '2000, PP1700'; 2000
[24] Ou X, Cakmak M. Polymer 2008;49:5344.
[25] Kokturk G, Cakmak M. Polym Eng Sci 2002;42:1619.
[26] Stein RS. In: Ke B, editor. Newer methods of polymer charaterization. New York: Intersecience Publishers; 1964.
[27] Ohkoshi Y, Shirai Hirohiko. Sen'i Gakkaishi 1999;55:62.
[28] Pae KD, Sauer JA. J Appl Polym Sci 1968;12:1901.
[29] O'Kane W, Young J, Ryan J, Bras W. Polymer 1994;35:1352.
[30] Toda T, Yoshida H, Fukunishi K. Polymer 1995;36:699.
[31] Jabarin SA. Polym Eng Sci 1991;131:1071.
[32] Peng KL, Roland CM. J Polym Sci Phys Ed 1993;vol 31:1339.